PHYSICAL REVIEW B VOLUME 2, NUMBER 10 15 NOVEMBER 1970

Numerical Study of Deformation-Potential Scattering of Electrons by Optical Phonons in a Longitudinal Magnetic Field

Robert L. Peterson
National Bureau of Standards, Boulder, Colorado 80302

and

*Microwave Department, Royal Institute of Technology, Stockholm, Sweden**
(Received 3 June 1970)

A detailed numerical study of the influence of a longitudinal magnetic field on carrier scattering is presented for the simple model of the band structure of a semiconductor and for deformation-potential scattering of carriers by optical phonons. A drifted Maxwellian distribution is used, and parallel electric and magnetic fields of arbitrary magnitude are considered. Interesting results of this study include magnetic-field-induced negative differential mobility, magnetic-field-induced "runaway" in the quantum limit, although not for ordinarily large magnetic fields, and longitudinal magnetoresistance resonances whose amplitudes are quite sensitive to electric field strength.

I. INTRODUCTION

Although much analytical work has been done on galvanomagnetic effects in semiconductors, numerical studies are not yet very extensive. In part, this is no doubt due to the fact that real semiconductors are usually very complicated, containing several anisotropic carrier bands and several simultaneously active scattering mechanisms for the carriers. This makes it very difficult to derive an accurate velocity distribution function, and perhaps discourages workers from making extensive numerical analyses.

However, in idealized cases one can go far with numerical studies, which can be very profitable for the insights they lead to, although they can be applied to real semiconductors only with great caution. We present here one such study, that of deformation-potential scattering of carriers by optical phonons ("nonpolar optical" scattering). This mechanism is present in all semiconductors, but is often dominated by other scattering mechanisms, depending upon lattice temperature, electric field strength, impurity content, and material. We assume a single carrier band with spherical energy surfaces and a parabolic dispersion relation, and consider parallel electric and magnetic fields of arbitrary magnitude. We further assume nondegenerate statistics and use the drifted-Maxwellian distribution,[1] that is, a distribution with two adjustable parameters (drift velocity and electron temperature) which are determined self-consistently. We do not wish to enter here upon a discussion of the relative merits and faults of this distribution, which are discussed elsewhere,[1] but rather to determine in some detail what such a distribution predicts about the influence of a magnetic field upon electrical transport. The advantage of the drifted Maxwellian of course is that it is relatively easy to use. It can be justified at sufficiently high carrier concentration.[2-4] Even when not strictly justifiable theoretically, it can provide a good description of experimental results.[5] The history of GaAs provides an interesting example of this.[6-11]

Although it is not the purpose of this paper to describe a real material, we may note that p-type germanium, with its almost parabolic, rather spherical, heavy-hole band and predominance of nonpolar optical phonon scattering,[12] is not too far removed from our model.

The theoretical basis for the calculations is standard and given briefly in Sec. II. Quantum-mechanical language is used, since large magnetic fields are considered. Section III contains analytical results applicable to various limiting situations. The numerical results, obtained by computer, are given in Sec. IV. These results include magnetic-field-induced negative differential mobility occurring for two different reasons and longitudinal magnetoresistance resonance structure which can be quite pronounced. Physical discussions of such effects are given, which are to a large extent independent of the distribution function we have used.

II. THEORETICAL BASIS

The interaction V describing deformation-potential scattering of a carrier (electrons or holes) by optical phonons is

$$V=\sum \overline{q}\, b_q\, e^{i\vec{q}\cdot\vec{r}}+\text{Hermitian conjugate}, \qquad (1)$$

where b_q is the phonon destruction operator for mode $\vec{q}$; $\vec{r}$ is the carrier position; the summation is over all longitudinal optical phonons; and $\overline{q}$ is the coupling constant, whose absolute square is given by[13]

$$|\overline{q}|^2=E_{1op}^2\hbar\omega_0/(2\Omega\rho u^2); \qquad (2)$$

Ω is the volume and ρ the mass density of the crys-

tal; u is the longitudinal speed of sound; ω_0 is the angular frequency of the optical phonons; and E_{1op} is a parameter with units of energy. The fact that $|\bar{q}|^2$ is independent of phonon wave vector $\vec{q}$, together with the assumption of dispersionless optical phonon modes, makes nonpolar optical scattering perhaps the simplest of all mechanisms to treat, particularly when a magnetic field is considered.

We treat the $H=0$ and $H\neq 0$ cases separately, considering first the case of zero magnetic field. The Hamiltonian for a carrier having effective mass m^* and momentum $\vec{p}=\hbar\vec{k}$, in an electric field $\vec{E}$ in the z direction, is

$$\mathcal{H}=p^2/2m^*+\mathcal{H}_L+V-eEz\ , \tag{3}$$

where $\mathcal{H}_L$ is the lattice Hamiltonian and V is the carrier-lattice interaction. In the steady state, the equations of motion for the average carrier momentum and energy are

$$\frac{d}{dt}\langle p_z\rangle = 0 = eE + \mathrm{Tr}\left(p_z \left.\frac{\partial\rho}{\partial t}\right|_{\mathrm{scat}}\right), \tag{4}$$

$$\frac{d}{dt}\left\langle\frac{p^2}{2m^*}\right\rangle = 0 = \frac{eE}{m^*}\langle p_z\rangle + \mathrm{Tr}\left(\frac{p^2}{2m^*}\left.\frac{\partial\rho}{\partial t}\right|_{\mathrm{scat}}\right), \tag{5}$$

in a quantum-mechanical notation. In Eqs. (4) and (5), $\partial\rho/\partial t|_{\mathrm{scat}}$ is the rate of change of the density matrix due to scattering. In the usual harmonic-lattice carrier–plane-wave basis, only the diagonal elements of ρ (i.e., the distribution function) are needed. Their rate of change due to scattering is given by the standard equation[14]

$$d\langle n,\vec{k}|\rho|n,\vec{k}\rangle/dt = \sum_{n',\vec{k}'} W_{n\vec{k},n'\vec{k}'}\left[\rho_{1\mathrm{att}}(n')\rho_{\mathrm{ca}}(\vec{k}') - \rho_{1\mathrm{att}}(n)\rho_{\mathrm{ca}}(\vec{k})\right], \tag{6}$$

where n represents all the phonon quantum numbers, and $|\vec{k}\rangle$ the carrier–plane-wave states. $W_{n\vec{k},n'\vec{k}'} = W_{n'\vec{k}',n\vec{k}}$ is the usual transition probability per unit time. For the lattice in thermal equilibrium at temperature T_0, sums over the phonon occupation numbers give Planck factors describing the number of thermal phonons in mode $\vec{q}$:

$$\bar{n}_q = [\exp(\hbar\omega_q/kT_0)-1]^{-1}\ . \tag{7}$$

The carrier distribution function $\rho_{\mathrm{ca}}(\vec{k})=\langle\vec{k}|\rho_{\mathrm{ca}}|\vec{k}\rangle$ is given the drifted-Maxwellian form

$$\rho_{\mathrm{ca}}(\vec{k}) = \Omega^{-1}(2\pi\beta\hbar^2/m^*)^{3/2}\exp[-\beta\hbar^2(\vec{k}-\bar{\vec{k}})^2/2m^*], \tag{8}$$

where $\hbar\bar{\vec{k}}=m^*\bar{v}=\langle\vec{p}\rangle$. The drift velocity of the carriers is denoted by $\bar{v}$, and their temperature by $T=1/k\beta$.

It is now simple and straightforward to obtain the two coupled integral equations determining $\bar{v}$ and T. We illustrate briefly with the momentum equation. Combining Eqs. (4) and (6), one obtains

$$\begin{aligned} eE &= \hbar\sum_{n,n'}\sum_{\vec{k},\vec{k}'}(k_z'-k_z)W_{n\vec{k},n'\vec{k}'}\rho_{1\mathrm{att}}(n')\rho_{\mathrm{ca}}(\vec{k}') \\ &= 2\pi|\bar{q}|^2\sum_{\vec{k},\vec{k}'}\sum_{\vec{q}}(k_z'-k_z)\rho_{\mathrm{ca}}(k')\{(\bar{n}_0+1)\delta_{\vec{k},\vec{k}'-\vec{q}} \\ &\quad\times\delta[\hbar^2(k^2-k'^2)/2m^*+\hbar\omega_0] + \bar{n}_0\delta_{\vec{k},\vec{k}'+\vec{q}} \\ &\quad\times\delta[\hbar^2(k^2-k'^2)/2m^*-\hbar\omega_0]\}. \end{aligned} \tag{9}$$

It is easiest to sum first over $\vec{q}$ for the nonpolar optical scattering mechanism. Doing this, then integrating on $\vec{k}$, using $\bar{n}_0+1=\bar{n}_0\exp(\gamma_0)$ where $\gamma_0=\beta_0\hbar\omega_0$, one gets

$$eE = \frac{|\bar{q}|^2\Omega m^*\bar{n}_0}{\pi\hbar^2}\sum_{\vec{k}'}k_z'\rho_{\mathrm{ca}}(\vec{k}') \times\left[e^{\gamma_0}\left(k'^2-\frac{2m^*\omega_0}{\hbar}\right)^{1/2}+\left(k'^2+\frac{2m^*\omega_0}{\hbar}\right)^{1/2}\right]. \tag{10}$$

Summation on $\vec{k}'$ is restricted in the first term (phonon emission) to $\vec{k}'$ values for which the radical is real. Integration over the angles in $\vec{k}'$ space completes this part of the analysis. The energy-transfer equation is handled in a very similar manner. Thus we obtain from the momentum and energy equations

$$\text{momentum:}\quad vE/E_{np} = \gamma^{1/2}\bar{n}_0 I_m\exp(-\gamma v^2), \tag{11}$$

$$\text{energy:}\quad vE/E_{np} = \gamma^{3/2}\bar{n}_0 I_e\exp(-\gamma v^2). \tag{12}$$

Equating the right-hand sides of these equations gives

$$\gamma I_e = I_m\ . \tag{13}$$

We have introduced the definitions

$$\gamma = \hbar\omega_0/kT = \theta/T\ , \tag{14}$$

$$\gamma_0 = \hbar\omega_0/kT_0 = \theta/T_0\ , \tag{15}$$

$$v = [\tfrac{1}{2}m^*\bar{v}^2/\hbar\omega_0]^{1/2}\ , \tag{16}$$

$$E_{np} = 2(E_{1op}m^*\hbar\omega_0)^2/(\pi^{3/2}\rho u^2\hbar^4 e)\ , \tag{17}$$

$$I_m = \int_0^\infty dx\, e^{-\gamma x^2}x^2(x^2+1)^{1/2}\{e^{\gamma_0-\gamma}[\cosh(2\gamma v(x^2+1)^{1/2}) - \sinh(2\gamma v(x^2+1)^{1/2})/(2\gamma v(x^2+1)^{1/2})] + \cosh(2\gamma vx) - \sinh(2\gamma vx)/(2\gamma vx)\}, \tag{18}$$

$$I_e = \int_0^\infty dx\, e^{-\gamma x^2}x^2(x^2+1)^{1/2}\{e^{\gamma_0-\gamma}\sinh[2\gamma v(x^2+1)^{1/2}]/[2\gamma v(x^2+1)^{1/2}] - \sinh(2\gamma vx)/(2\gamma vx)\}. \tag{19}$$

Equation (13) is a desirable equation to use since E is eliminated from it. For given v, one may calculate γ from Eq. (13) and use this pair of values in Eq. (11) to calculate E/E_{np}.

Next we turn to the case of nonzero $\vec{H}$. We take $\vec{H}$ parallel to $\vec{E}$ and in the z direction. With the usual choice of vector potential ($A_x = A_z = 0$, $A_y = xH$), the carrier Hamiltonian is[15]

$$\mathcal{H}_{ca} = (\vec{p} - e\vec{A}/c)^2/2m^* = [p_x^2 + p_z^2 + (p_y - m^*\omega x)^2]/2m^*, \tag{20}$$

where

$$\omega = eH/m^*c \tag{21}$$

is the cyclotron frequency. The transverse part of the Hamiltonian (20) can be transformed into harmonic oscillator form (Landau quantization), giving for the carrier energy

$$E_{ca}(k_z, m) = k_z^2/2m^* + \hbar\omega(m + \tfrac{1}{2}). \tag{22}$$

The Landau levels are denoted by index $m = 0, 1, 2, \ldots$. There is an energy degeneracy which may be associated with the y degree of freedom.

Fortunately, one does not need to deal explicitly with the harmonic oscillator wave functions when considering nonpolar optical scattering, because of the "sum rule" due to Titeica.[16] Thus, using plane-wave states for the y and z directions, one has

$$\langle m' k_y' k_z' | e^{\pm i\vec{q}\cdot\vec{r}} | m k_y k_z \rangle = \delta_{\pm q_y, k_y' - k_y}\, \delta_{\pm q_z, k_z' - k_z} \times J^{\pm}_{m'm}(q_x, k_y', k_y), \tag{23}$$

where

$$J^{\pm}_{m'm}(q_x, k_y', k_y) = \int_{-\infty}^{\infty} dx\, e^{\pm i q_x x} u^*_{m'}(x + k_y'/2\alpha) \times u_m(x + k_y/2\alpha), \tag{24}$$

$$\alpha = m^*\omega/2\hbar\,. \tag{25}$$

The Titeica sum rule, easily proved,[16,17] is

$$\int_{-\infty}^{\infty} dq_x \int_{-\infty}^{\infty} dq_y \left| J^{\pm}_{m'm}(q_x, k_y \pm q_y, k_y) \right|^2 = 4\pi\alpha\,. \tag{26}$$

The drifted-Maxwellian distribution function now takes the form

$$\rho_{ca}(m k_y k_z) = \rho_m \rho(k_y k_z), \tag{27}$$

where

$$\rho_m = \exp(-\beta\hbar\omega m)\,[1 - \exp(-\beta\hbar\omega)], \tag{28}$$

$$\rho(k_y k_z) = (N_y L_z)^{-1} (2\pi\beta\hbar^2/m^*)^{1/2} \times \exp[-\beta\hbar^2(k_z - \bar{k})^2/2m^*]\,. \tag{29}$$

N_y is the number of degrees of freedom associated with the y direction, and L_z is the length of the sample in the z direction.

We shall also use the result

$$\sum_{m, m'=0}^{\infty} \rho_{m'} f(m - m') = \sum_{l=0}^{\infty} f(l) + \sum_{l=1}^{\infty} f(-l) \exp(-\beta\hbar\omega l)\,, \tag{30}$$

where $f(m - m')$ is an arbitrary function of the difference $m - m'$. This is easily proved by resumming the left-hand side as

$$\sum_{l=0}^{\infty} f(l) + \sum_{l=1}^{\infty} f(-l) \sum_{m=l}^{\infty} \rho_m\,,$$

and noting that

$$\sum_{m=l}^{\infty} \rho_m = \rho_l/[1 - \exp(-\beta\hbar\omega)]\,.$$

We now proceed as before, writing the equations of motion for p_z and $\mathcal{H}_{ca}$, imposing the steady-state condition, summing first over phonon numbers, then on $\vec{q}$, k_y', k_y, and k_z, using Eq. (26). With the summation theorem [Eq. (30)] we finally obtain

$$\text{momentum:}\quad vE/E_{np} = \gamma^{1/2}\bar{n}_0 I_m(H) \exp(-\gamma v^2), \tag{31}$$

$$\text{energy:}\quad vE/E_{np} = \gamma^{3/2}\bar{n}_0 I_e(H) \exp(-\gamma v^2)\,. \tag{32}$$

Equating the right-hand sides of Eqs. (31) and (32), we have

$$\gamma I_e(H) = I_m(H)\,. \tag{33}$$

We use Eqs. (31) and (33) in computing. The H-dependent collision integrals are given by

$$I_m(H) = \frac{v\omega}{2\omega_0} \int_0^{\infty} dx \exp(-\gamma x^2) \left[\sum_{l=0}^{\infty} S(x_l^+, x) \exp\left(-l\gamma\frac{\omega}{\omega_0}\right) \Big/ x_l^+ + \sum_{l\omega > \omega_0} S(x, x_l^-) \exp\left(\gamma - l\gamma\frac{\omega}{\omega_0}\right) \Big/ x_l^- + \sum_{l=1}^{l\omega \le \omega_0} S(x_{-l}^+, x)/x_{-l}^+ \right], \tag{34}$$

$$I_e(H) = \frac{\omega}{4\gamma\omega_0} \int_0^{\infty} dx \exp(-\gamma x^2) \left[\sum_{l=0}^{\infty} C(x_l^+, x) \exp\left(-l\gamma\frac{\omega}{\omega_0}\right) \Big/ x_l^+ + \sum_{l\omega > \omega_0}^{\infty} C(x, x_l^-) \exp\left(\gamma - l\gamma\frac{\omega}{\omega_0}\right) \Big/ x_l^- + \sum_{l=1}^{l\omega \le \omega_0} C(x_{-l}^+, x)/x_{-l}^+ \right], \tag{35}$$

where

$$S(x, y) = e^{\gamma_0 - \gamma}\, x \sinh(2\gamma v x) + y \sinh(2\gamma v y), \tag{36}$$

$$C(x, y) = e^{\gamma_0 - \gamma} \cosh(2\gamma v x) - \cosh(2\gamma v y), \tag{37}$$

$$x_l^{\pm} = (x^2 + l\omega/\omega_0 \pm 1)^{1/2}\,. \tag{38}$$

This completes the development of the basic equations.

III. ANALYTICAL RESULTS

For arbitrary H, the average energy of a carrier is, from Eqs. (27)–(29),

$$\langle \mathcal{E} \rangle_H = \tfrac{1}{2}m^*\bar{v}^2 + \tfrac{1}{2}kT + \tfrac{1}{2}\hbar\omega \coth(\hbar\omega/2kT). \quad (39)$$

At $H=0$, this becomes

$$\langle \mathcal{E} \rangle_0 = \tfrac{1}{2}m^*\bar{v}^2 + \tfrac{3}{2}kT\,, \quad (40)$$

which of course also follows from Eqs. (8) and (9).

Paranjape[18] first pointed out that the electron temperature need not rise above the lattice temperature upon application of an electric field, which is evident upon comparing Eqs. (39) or (40) with their $E=0$ counterparts. He also showed that for both polar and nonpolar optical phonon scattering at $H=0$, the electron temperature would initially fall, provided the lattice temperature was below a certain critical value. We shall briefly rederive this result below for nonpolar optical scattering, in order to compare it with the quantum-limit case.

Magnusson and Weissglas[19] showed, for polar materials, that in the quantum limit the electron temperature would initially decrease much more rapidly than at $H=0$ because only one degree of freedom can absorb the random energy. This is readily seen also from Eq. (39): since the coth term is quite slowly varying in the quantum limit ($\hbar\omega \gg kT$), the change of energy upon application of the electric field is approximately

$$\tfrac{1}{2}m^*\bar{v}^2 + \tfrac{1}{2}k(T - T_0),$$

as compared with

$$\tfrac{1}{2}m^*\bar{v}^2 + \tfrac{3}{2}k(T - T_0)$$

at $H=0$. Thus, if the energy given to the drift term is roughly the same in the two limits (and it is, except at large E), the temperature change $|T - T_0|$ will be about three times greater in the quantum limit, for any scattering mechanism.

Consider $H=0$. At low E, $\delta = \gamma_0 - \gamma$ is of the order of v^2. Expanding I_m and I_e [Eqs. (18) and (19)] to terms of this order, one finds

$$I_m = \tfrac{1}{3}\gamma_0 v^2 e^{\gamma_0/2} K_2(\tfrac{1}{2}\gamma_0)\,, \quad (41)$$

$$I_e = \tfrac{1}{12}(3\delta + 2\gamma_0^2 v^2) e^{\gamma_0/2} K_1(\tfrac{1}{2}\gamma_0). \quad (42)$$

Properties of the modified Bessel functions K_n may be found in Ref. 20. Equation (13) may then be written as

$$\gamma = \gamma_0 + \tfrac{1}{3}\gamma_0 v^2 \left[\tfrac{1}{2}\gamma_0 - \frac{K_2(\frac{1}{2}\gamma_0)}{K_1(\frac{1}{2}\gamma_0)}\right]. \quad (43)$$

Recalling the definitions of γ and γ_0 [Eqs. (14) and (15)], one thus sees that the electrons are cooled at sufficiently small E if $K_2(\frac{1}{2}\gamma_0) < (\frac{1}{2}\gamma_0)K_1(\frac{1}{2}\gamma_0)$, or $\gamma_0 \gtrsim 3.75$, or $T_0 \lesssim 0.267\,\theta$.

Some physical discussion of this result is in order. By keeping track of the emissive and absorptive terms, one sees that spontaneous emission of optical phonons makes no contribution to the momentum transfer, to order v^2. Equation (41) results from approximately equal portions of absorption and stimulated emission, biased somewhat toward emission especially at the lower lattice temperatures. Energy gain by the carriers by absorption is completely canceled by stimulated emission to order v^2. The net energy transfer is both by spontaneous emission [the δ term in Eq. (42)] and stimulated emission (the v^2 term).

One can understand why the electron temperature initially decreases at sufficiently low lattice temperature in the drifted-Maxwellian formulation. As the distribution function drifts toward positive $\vec{k}$, the number of carriers of positive $\vec{k}$ sufficiently energetic to emit an optical phonon tends to increase, and these then scatter efficiently back to near $\vec{k}=0$, so that the forward tail of the distribution tends to shorten. The backward tail, however, is not much affected. Thus the actual distribution function tends to become skewed unless the carrier concentration is sufficiently high. The net effect is a narrower distribution, which in the drifted-Maxwellian picture requires a lower temperature. At higher lattice temperatures, absorption and stimulated emission processes become more important, so that the carriers in the central portions of the distribution function become active, negating the tendencies just mentioned.

The zero-field mobility $\mu_0 = \bar{v}/E$, $E \to 0$, is obtained from the momentum equation (11) together with Eq. (41):

$$\mu_0 = \left[\frac{72k^3T_0^3}{E_{np}^2 m^* \hbar^2 \omega_0^2}\right]^{1/2} \frac{\sinh(\hbar\omega_0/2kT_0)}{K_2(\hbar\omega_0/2kT_0)}\,, \quad (44)$$

a result obtained by Sato[21] with the drifted Maxwellian.

An interesting question is whether the drift velocity saturates at large E and $H=0$. That it does has been established by Barrie and Burgess[22] using a drifted-Maxwellian approach, and by Sato[21] with a non-Maxwellian technique. The limiting value determined by these two approaches is, interestingly, the same. It may be found by considering Eqs. (18) and (19) as $T \to \infty$. Noting that the major contributions to the integrals occur at $x \gg 1$, one finds for large E

$$I_m = (4v^2/3\gamma)[\exp(\gamma_0) + 1]\,,$$

$$I_e = (1/2\gamma^2)[\exp(\gamma_0) - 1]\,,$$

so that Eq. (13) becomes

$$v_{\lim}^2 = \tfrac{3}{8}\tanh(\theta/2T_0)\,. \quad (45)$$

For $T_0 \ll \theta$, one thus finds $v_{\text{lim}} \approx 0.61$, or $(m^*\bar{v}^2/2)_{\text{lim}} = \frac{3}{8}\hbar\omega_0$. The limiting drift energy at low temperatures thus depends only upon the optical phonon energy.

It has been established[23,24] that runaway *does* occur for polar optical scattering at $H=0$. The reason for the difference from nonpolar optical scattering is that in the latter, the scattering frequency [Eq. (2)], is constant, whereas in polar optical scattering it varies as q^{-2}, where q is phonon wave number. Thus, the large momentum transfer required for optical phonon emission and absorption is severely inhibited in the polar case, and this reduced scattering probability permits the carrier runaway.

We turn now to the $H \neq 0$ case. First, it is important to know that these equations reduce in the limit $H \to 0$ to their $H=0$ analogs. The procedure is simple but quite tedious; we will not demonstrate it here. One uses the continuous variable $l\omega/\omega_0$ in this limit and performs one integration in each term of the collision integrals. Transformations of variable, interchanges of integration order, and integration by parts are required. Thus one can show that

$$\lim I_m(H) = I_m, \quad \lim I_e(H) = I_e . \tag{46}$$

The quantum limit, defined by $\hbar\omega \gg kT$, is of considerable interest. In this limit the collision integrals are, from Eqs. (34)–(38),

$$I_m(H\to\infty) = (v\omega/2\omega_0)\int_0^\infty dx \exp(-\gamma x^2) S(x_0^+, x)/x_0^+, \tag{47}$$

$$I_e(H\to\infty) = (\omega/4\gamma\omega_0)\int_0^\infty dx \exp(-\gamma x^2)\, C(x_0^+, x)/x_0^+ . \tag{48}$$

Equation (33) thus becomes independent of H as well as of E, and a unique T, $\bar{v}$ relationship obtains, as with $H=0$. Also of interest in this limit is the effect of the magnetic field upon the lattice temperature at which electron cooling can occur. To terms of order v^2, one finds

$$I_m(H\to\infty) = (v^2\omega/2\omega_0)\gamma_0 e^{\gamma_0/2} K_1(\tfrac{1}{2}\gamma_0) , \tag{49}$$

$$I_e(H\to\infty) = (\omega/8\gamma_0\omega_0)(\delta + 2\gamma_0^2 v^2) e^{\gamma_0/2} K_0(\tfrac{1}{2}\gamma_0) . \tag{50}$$

Equation (33) then becomes

$$\gamma = \gamma_0 + 4\gamma_0 v^2[\tfrac{1}{2}\gamma_0 - K_1(\tfrac{1}{2}\gamma_0)/K_0(\tfrac{1}{2}\gamma_0)], \tag{51}$$

which may be compared with Eq. (43). Initial cooling occurs if $K_1(\frac{1}{2}\gamma_0) < \frac{1}{2}\gamma_0 K_0(\frac{1}{2}\gamma_0)$, or $\gamma_0 \gtrsim 2.61$, or $T_0 \lesssim 0.38\theta$. The effect of the strong magnetic field is thus to raise by more than 40% the lattice temperature at which initial electron cooling is possible.

The zero-field mobility in the quantum limit is obtained by combining Eqs. (31) and (49):

$$\mu_0(H\to\infty) = \left[\frac{32k^3T_0^3}{E_{np}^2 m^* \hbar^2\omega^2}\right]^{1/2} \frac{\sinh(\hbar\omega_0/2kT_0)}{K_1(\hbar\omega_0/2kT_0)} . \tag{52}$$

The quantum-limit mobility is thus inversely proportional to magnetic field.

The ratio of the quantum limit to $H=0$ mobilities is simply

$$\frac{\mu_0(H\to\infty)}{\mu_0(H=0)} = \frac{2}{3}\,\frac{\omega_0}{\omega}\,\frac{K_2(\theta/2T_0)}{K_1(\theta/2T_0)} . \tag{53}$$

(The modified Bessel functions become asymptotically equal at large argument, i.e., at $T_0 \ll \theta$.)

In contrast to the $H=0$ case, the drift velocity does not saturate in the quantum limit. In fact, the strong magnetic field induces runaway, that is, at a certain value of E, the slope $d\bar{v}/dE$ becomes infinite. By reducing the carrier density of states at large carrier energies, the magnetic field reduces the scattering cross section by optical phonon emission to such an extent that the emitted phonons cannot carry away energy fast enough to prevent a runaway of the drift energy of the carriers. (Of course, other scattering mechanisms would control the drift velocity at that point.) The physical discussion in the two paragraphs following Eq. (43) for $H=0$ apply in the quantum limit as well. The magnetic field also induces negative differential mobility at E values less than the value for runaway, provided the lattice temperature is sufficiently low. This is discussed further and illustrated in Sec. IV.

Finally, we come to the region of intermediate magnetic field, which is the most difficult region to treat, both analytically and numerically. Notice that the energy collision integral [Eq. (35)], contains some apparently divergent terms at resonance, i.e., $l\omega = \omega_0$. (This is not true for the momentum collision integral.) The $\vec{k}=0$ carriers give rise to the singularities. We can use these terms to show that at resonance, the carrier temperature must return to the lattice temperature, whether it has been above or below it off resonance. Thus, if the magnetic field is just off resonance, Eq. (35) can be written

$$I_e(H) = R(e^{\gamma_0-\gamma} - 1)/\gamma + \text{well-behaved terms}, \tag{54}$$

where R is of large magnitude, increasing without bound as resonance is approached. Equation (33) together with Eq. (34), however, shows that $\gamma I_e(H)$ must be finite at resonance. Thus Eq. (54) requires that $T \to T_0$. That is, the distribution function will broaden if the carriers were cool, or narrow if the carriers were hot, as the magnetic field sweeps through a resonance. This result, together with the shifting of the mean of the distribution at resonance, has interesting implications for acoustic amplification, which is sensitive to the shape of the distribution function near $\vec{k}=0$.[25]

IV. NUMERICAL RESULTS AND DISCUSSION

Equations (13) and (33), which combine the energy

and momentum equations, are independent of E, so that a unique velocity-temperature relationship exists. Moreover, in the quantum limit, as seen from Eq. (33) together with Eqs. (47) and (48), this relationship is independent of H as well. We show the $H=0$ and quantum-limit curves in Fig. 1 for $T_0=\frac{1}{8}\theta$. We also give curves at the critical temperatures (the lattice temperature below which initial electron cooling can occur): $T_0=\theta/3.75$ at $H=0$ and $T_0=\theta/2.61$ in the quantum limit. The cooling effect with increasing drift velocity (or, in other words, the narrowing of the distribution function as it moves to the right) is seen at the lower temperature, and is quite pronounced in the quantum limit. When the reduced velocity [see Eq. (16)] reaches about 0.45 at $T_0=\frac{1}{8}\theta$, the electron temperature increases rapidly (the distribution function rapidly broadens while its mean value shifts little). The drift velocity then saturates as the temperature becomes infinite at $H=0$, but increases indefinitely with increasing temperature in the quantum limit. The quantum-limit low-temperature curve also shows a region of decreasing drift velocity with increasing temperature. This is connected with a region of negative differential mobility, as is seen in subsequent figures.

Figure 2 shows the variation of drift velocity with electric field for $H=0$, H near the first resonance ($\omega\approx\omega_0$), and the quantum limit. The logarithmic E scale used emphasizes the low and intermediate regions of electric field (Ohm's law is an exponentially increasing curve on such a plot). Figure 2 reveals at $T_0=\frac{1}{8}\theta$ and $H=0$, a "precursor" plateau occurring prior to saturation. The same effect is seen also at the higher temperature of $T_0=\theta/3.75$ as a nearly linear region. These precursors begin at the electric field for which the electron temperature begins increasing (see Fig. 5). The quantum-limit curve at $T_0=\frac{1}{8}\theta$ shows the precursor plateau to have developed into a region of negative differential mobility (ndm), followed by runaway before the final plateau can be achieved. At the higher temperature $T_0=\theta/2.61$, there is no quantum limit ndm, and runaway occurs at about the same value of electric field as the lower temperature. Notice that in the quantum limit, the external parameter is the combination E/H (the quantum-limit scale is at the top of Fig. 2); runaway occurs at $(E/E_{np})/(\omega/\omega_0)\approx 0.21$. For the curve near resonance, the initial mobility is smaller than at $H=0$, but greater than in the quantum limit. However, the drift velocity rises to a considerably higher maximum value, before finally decreasing in a region of ndm.

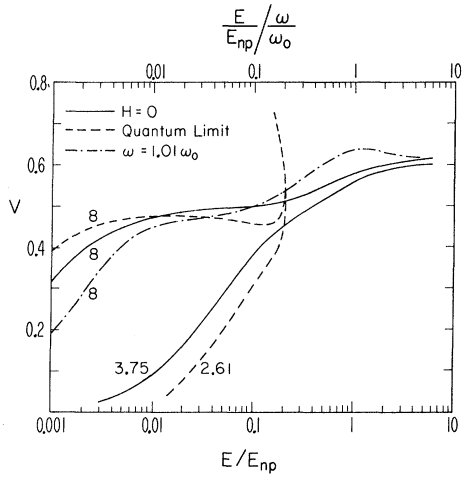

FIG. 2. Variation of reduced drift velocity with reduced electric field (semilog plot) for $H=0$, H near the first resonance, and H in the quantum limit. Scale at top refers to quantum limit. Numbers on curves give values of θ/T_0.

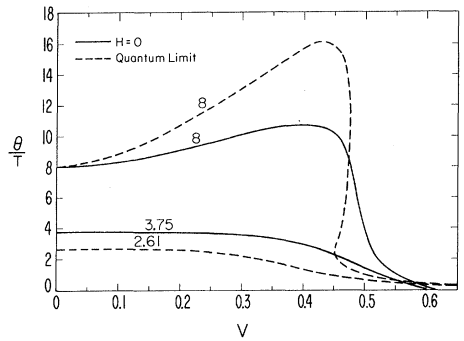

FIG. 1. Variation of inverse electron temperature with reduced drift velocity. Numbers on curves give values of θ/T_0.

In Fig. 3, we again show the dependence of drift velocity upon field, this time on a linear E scale, at the low temperature $T_0=\frac{1}{8}\theta$, and several values of magnetic field. Apart from the curves close to resonance, these curves show the progressive development of ndm with increasing magnetic field. Although the ndm can begin at electron temperatures somewhat below the lattice temperature, in the main it is connected with the higher electron temperatures. Upon further increase of electric field, the drift velocity rises to a saturation value. Notice that even at the extremely high magnetic field corresponding to $\omega=10\omega_0$, electron runaway does not occur (the quantum-limit condition is violated before runaway occurs), although a rather sharp increase in drift velocity takes place, followed by saturation. Two curves near resonance are also shown, at $\omega/\omega_0=1+10^{-2}$ and $1+10^{-5}$. Although the maximum drift velocity rises considerably as resonance is approached, of more significance is the

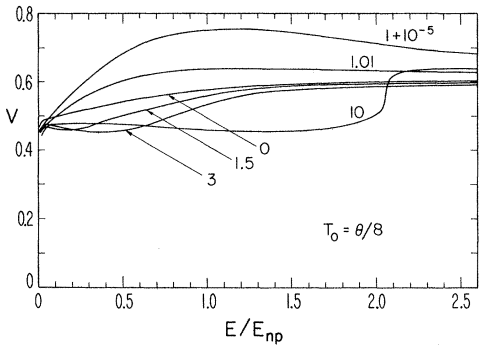

FIG. 3. Variation of reduced drift velocity with reduced electric field at $T_0 = \frac{1}{8}\theta$ (both scales linear). Numbers on curves give values of ω/ω_0.

narrowness of the span of H for which this increase is large. Thus there can be a considerable negative magnetoresistance near the resonance points in the hot-electron region, but the "linewidth" is small.

The nonresonant magnetic-field-induced ndm is a low-temperature phenomenon. In Fig. 4 we show the $\omega/\omega_0 = 0$, $1+10^{-5}$, and 10 curves for $T_0 = \frac{1}{5}\theta$. At this temperature, the ndm at very large magnetic field has vanished, leaving a very flat portion in the $\overline{v} - E$ characteristic. There is still a sharp increase in drift velocity, however, toward the saturation value, at about the same electric field as at lower temperature. The resonance curve, however, is quite similar to that at the lower temperature, differing principally in the low-E region. The maximum velocity and degree of ndm are not changed materially.

Perhaps we should mention at this point that for finite H, the computer was allowed to sum over as many Landau levels as necessary to achieve the specified accuracy; our criterion was that for each point in the integration in the collision integrals, summation over Landau levels would continue until a term was reached whose contribution to the integrands was less than 10^{-3} in magnitude of the sum of the preceding contributions.

The features seen in Figs. 2–4 can be understood on physical grounds. (One must recognize of course that the finer details, such as the difference between a small ndm and a flat portion of the $\overline{v} - E$ characteristic, or the delicate balance between "restraint" and runaway, cannot usually be resolved by general physical arguments.) Consider first the "precursor" plateaus which appear at the lowest temperatures at $H = 0$ on the semilog plot. The prior decrease of electron temperature reflects the tendency of the number of "active" carriers (those capable of spontaneously emitting an optical phonon) to remain small, as discussed in Sec. III. When the electron temperature begins its rise, the backward scattering of active carriers increases first, producing the first elbow, i.e., the "precursor" plateau, in the $\overline{v} - E$ characteristic. However, as long as T is in the neighborhood of T_0, absorptive processes are not negligible and these dilute the backward scattering. When T is considerably greater than T_0, the emissive processes greatly predominate, and the net scattering probability increases, producing the final plateau.

It is evidently the high final density of states for the energetic carriers at $H = 0$ which tips the balance in favor of restraint rather than runaway. We mentioned above that in the quantum limit, the smaller density of states for energetic carriers makes runaway at large E understandable in this limit. At smaller E and low temperature, one can also understand why there is a tendency toward ndm. That is, T must increase more rapidly once past its minimum, in the quantum limit than at $H = 0$, as explained at the beginning of this section. The first effect is a strong increase in the backward scattering of active carriers, stronger than at $H = 0$, and leading to ndm. As T continues to rise, forward scattering begins to occur; since the mean of the distribution is closer to $k_z = 0$ than it is at $H = 0$, the forward scattering of active carriers at negative k_z now begins to play a more important role than at $H = 0$, reducing the scattering probability and contributing to the runaway.

The steplike behavior of the $\overline{v} - E$ characteristic at large E and very large but finite magnetic field is readily understood: at sufficiently large E, the electron temperature has become high enough that the most energetic carriers – those with energy greater than $2\hbar\omega_0$ – are able to scatter with high probability into the high density-of-states $k_z = 0$ region of the next-higher Landau level ($\Delta l = +1$ transitions). This scattering is sufficiently strong to

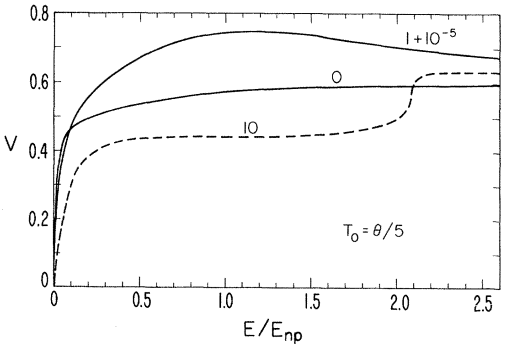

FIG. 4. Variation of reduced drift velocity with reduced electric field at $T_0 = \frac{1}{5}\theta$ (both scales linear). Numbers on curves give values of ω/ω_0.

prevent runaway.

The resonance curves are also understandable. Close to resonance, energy exchange is very efficient, but net energy transfer is very small at low E, because absorption and stimulated emission involving "passive" carriers dominate, and the energy transfers are nearly canceled. In the language of temperature, one would say that the electron temperature changes little (as shown in Fig. 5). The principal effect is a shift of the distribution function to the right. The shift will be further than in the quantum limit because the forward scattering due to active carriers does not decrease as rapidly as in the quantum limit. This tendency persists to moderate values of E: resonance scattering keeps absorption and stimulated emission influential, and the drift velocity can rise to a high value. Finally, however, the large displacement of the distribution function combined with an increasing temperature brings about efficient back scattering of carriers of energy greater than $2\hbar\omega_0$ via $\Delta l = +1$ transitions, and, as it happens, the scattering is strong enough to produce ndm.

Figure 5 shows the variation of electron temperature with electric field at $H = 0$ and the quantum limit at $T_0 = \frac{1}{8}\theta$ and at the critical temperatures. We also show the temperature variation for the magnetic field near the first resonance: $\omega/\omega_0 = 1 + 10^{-5}$ for $T_0 = \frac{1}{8}\theta$. Clearly evident is the tendency of the electron temperature to remain closer to the lattice temperature than at nonresonant values.

In Fig. 6 we show the variation of electron temperature with magnetic field at $T_0 = \frac{1}{8}\theta$ and $\theta/3.75$, for several values of electric field outside the Ohmic region. Resonant structure, occurring when the optical phonon frequency is a multiple of the cyclotron frequency, is evident. As mentioned in Sec. III, the electron temperature rises toward the lattice temperature at resonance in the cool-electron region, and falls in the hot-electron region. The "linewidth" becomes very small as the lattice temperature is approached, and we have not continued the curves to the lattice temperature for this reason.

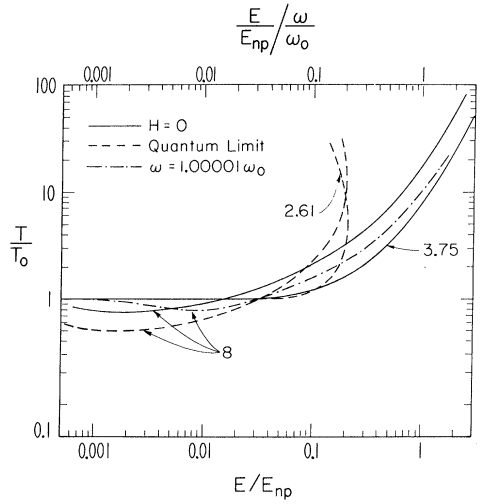

FIG. 5. Variation of reduced electron temperature with reduced electric field for $H = 0$, H very close to the first resonance, and H in quantum limit. Scale at top refers to quantum limit. Numbers on curves give values of θ/T_0.

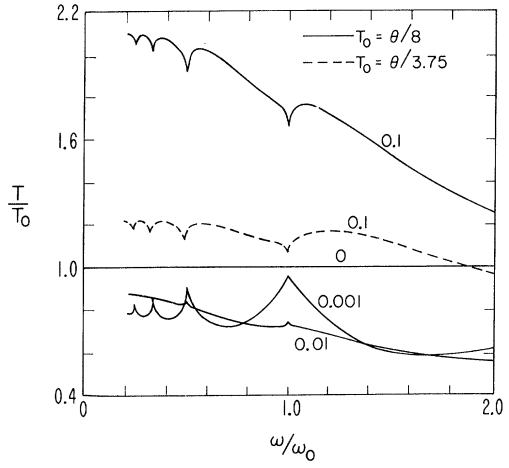

FIG. 6. Variation of reduced electron temperature with reduced magnetic field. Numbers on curves give values of E/E_{np}.

Figure 3 makes it evident that there is also a resonant structure in the longitudinal magnetoresistance. By the usual definition, we have

$$\frac{\Delta\rho}{\rho_0} = \frac{\rho(E, H)}{\rho(E, 0)} - 1 = \frac{\mu(E, 0)}{\mu(E, H)} - 1 \ . \tag{55}$$

The mobilities in Eq. (55) are defined as the ratio of drift velocity to electric field, rather than as differential mobilities. Thus the longitudinal magnetoresistance may also be written as

$$\frac{\Delta\rho}{\rho_0} = \frac{\overline{v}(E, 0)}{\overline{v}(E, H)} - 1 \approx \frac{\Delta v}{\overline{v}(E, 0)} \ . \tag{56}$$

The approximate equality in Eq. (56) results if $|\Delta v| = |\overline{v}(E, 0) - \overline{v}(E, H)| \ll \overline{v}(E, 0)$. Because of the appearance of $\overline{v}$ in the denominator, the conventional method of defining magnetoresistance tends to magnify structure at the lower values of $\overline{v}$, hence E, provided one is outside the Ohm's law region. This effect is evident in Fig. 7, in which magnetoresistance is plotted as a function of magnetic field strength. Curves are given for $E/E_{np} = 0$ and 0.1 at $T_0 = \theta/3.75$ (upper graph), and for $E/E_{np} = 0$, 0.001, 0.01, and 0.1 at $T_0 = \frac{1}{8}\theta$ (lower

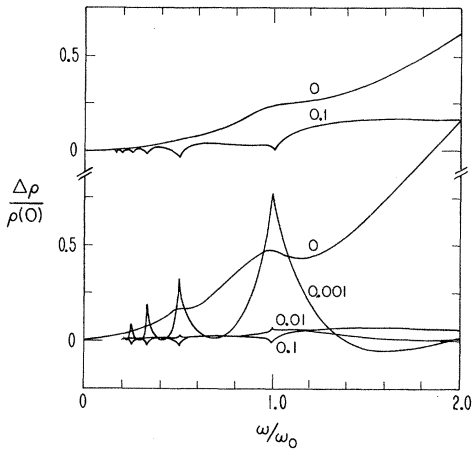

FIG. 7. Variation of longitudinal magnetoresistance with reduced magnetic field. Upper graph: $T_0=\theta/3.75$; lower graph: $T_0=\frac{1}{8}\theta$. Numbers on curves give values of E/E_{np}.

graph). (The 0.001 and 0.01 curves at $T_0=\theta/3.75$ lie quite close to the $E=0$ curve and are not plotted.)

The $E=0$ curves show the minor resonance structure which is now well known.[26] The 0.001 curve at $T_0=\frac{1}{8}\theta$ (which Fig. 2 confirms as in the non-Ohmic region) shows an unexpectedly large structure, which, however, is explained in large part by the argument in the preceding paragraph. At $E/E_{np}=0.01$ and $T_0=\frac{1}{8}\theta$, the resonant structure has largely vanished, although it reappears at $E/E_{np}=0.1$. Note also the regions of negative magnetoresistance, occurring near the resonance points when the electrons are hot, and near $\omega=1.5\omega_0$ for $E/E_{np}=0.001$ and $T_0=\frac{1}{8}\theta$.

Of interest is the fact that the "spikes" point up for some electric fields and down for others. This is related to the electron temperature: for temperatures below the lattice temperature, the spikes rise as resonance is approached, whereas if the electrons are hot, the spikes fall. The resonance structures in Fig. 7 are quite sharp because at the electric fields chosen, the electron temperature is distinctly different from the lattice temperature, except very close to resonance. However, for fields at about 0.02 E_{np}, the two temperatures are close (see Fig. 5) and the magnetoresistance curves do not necessarily have their extrema at the resonance points, and are then not cusplike. (Unpublished computations based on polar optical phonon scattering also show this.) Thus, optical phonon frequencies are not readily measurable from magnetoresistance structure, even for the simple model of band structure considered here, unless the electric field is properly chosen.

In conclusion, we have emphasized in this paper the temperature region for which T_0 is considerably smaller than the Debye temperature θ, because only at such temperatures do the more interesting effects discussed here occur. It should be kept in mind, however, that for $T_0\ll\theta$, other scattering mechanisms, for example, involving acoustic phonons or impurities, usually become dominant in real semiconductors. The pronounced magnetoresistance resonance structure and the negative differential mobility will both be diminished in magnitude by such scattering mechanisms. Nevertheless, it is important to understand what may be expected from each scattering mechanism separately.

The physical discussions we have given are to a large extent independent of the details of the distribution function used. In most instances "electron temperature" is simply a convenient way of referring to the width of the distribution. The principal unphysical aspect of the drifted Maxwellian, at low enough carrier concentrations that it cannot be justified, seems to us to be the restriction against skewness, or asymmetry about the mean. Forward scattering of active carriers in the negative-$\vec{k}$ region would then seem to be underestimated. Boardman, Fawcett, and Rees[11] drew a similar conclusion from comparing the drifted Maxwellian with a Monte Carlo technique. This implies that the restraining effects on the drift velocity would be somewhat smaller than given by the drifted Maxwellian. Nevertheless, the non-Maxwellian technique of Sato[21] predicts complete restraint at $H=0$ and gives precisely the same saturation velocity as the drifted Maxwellian; however, Sato assumed a symmetric distribution about the mean. Of course the details of the backward scattering are also not accurately handled at low carrier concentration, so it is difficult to make definitive statements in this region.

It is our opinion that a solution of the Boltzmann equation including nonpolar optical phonon scattering and carrier-carrier scattering would show, even at "moderate" carrier concentrations, the same general features found in this paper: complete restraint at $H=0$; runaway in the quantum limit preceded by a region of ndm if $T_0\ll\theta$; steplike behavior of the $\bar{v}-E$ characteristic at magnetic fields such that $\omega\gg\omega_0$, for $T_0\ll\theta$; and pronounced resonant structure, including ndm near resonance at large E.

ACKNOWLEDGMENTS

It is a pleasure to acknowledge the kind hospitality of the Microwave Department, Royal Institute of Technology, where this work was completed. I wish to thank Peter Weissglas and Bo Magnusson for helpful discussions and for reading the manuscript, and Bernice Bender for assistance with a portion of the programming.

*Temporary address.
[1]E. M. Conwell, in *Solid State Physics*, edited by F. Seitz, D. Turnbull, and H. Ehrenreich (Academic, New York, 1967), Suppl. 9, p. 14.
[2]H. Fröhlich and B. V. Paranjape, Proc. Phys. Soc. (London) B69, 21 (1956).
[3]R. Stratton, Proc. Roy. Soc. (London) A242, 355 (1957); *International Conference on Solid-State Physics, Brussels, June*, 1958 (Academic, New York, 1960), Vol. I, p. 343.
[4]A. Hasegawa and J. Yamashita, J. Phys. Soc. Japan 17, 1751 (1962).
[5]E. deAlba and V. V. Paranjape, Phys. Letters 11, 12 (1964).
[6]P. Butcher and W. Fawcett, Proc. Phys. Soc. (London) 86, 1205 (1965); Phys. Letters 21, 489 (1966).
[7]E. M. Conwell and M. O. Vassel, Appl. Phys. Letters 9, 411 (1966).
[8]J. G. Ruch and G. S. Kino, Appl. Phys. Letters 10, 40 (1967).
[9]B. Fay and G. S. Kino, Appl. Phys. Letters 15, 337 (1969).
[10]A. Sher and K. K. Thornber, Appl. Phys. Letters 11, 3 (1967).
[11]A. D. Boardman, W. Fawcett, and H. D. Rees, Solid State Commun. 6, 305 (1968).
[12]Reference 1, p. 59 ff.
[13]Reference 1, p. 150.
[14]Equation (6) is a special form of the Pauli master equation, used extensively in the quantum mechanics of the solid state. For example, it has recently been used in a theoretical study of transport in asymptotically high magnetic fields perpendicular to electric fields by H. F. Budd, Phys. Rev. 175, 241 (1968).
[15]W. Zawadski, in *Physics of Solids in Intense Magnetic Fields*, edited by E. D. Haidemenakis (Plenum, New York, 1969), p. 301.
[16]V. S. Titeica, Ann. Phys. (Paris) 22, 129 (1935).
[17]P. N. Argyres, J. Phys. Chem. Solids 4, 19 (1958).
[18]V. V. Parenjape and T. P. Ambrose, Phys. Letters 8, 223 (1964); V. V. Paranjape and E. de Alba, Proc. Phys. Soc. (London) 85, 945 (1965).
[19]B. Magnusson and P. Weissglas, Microwave Dept., Royal Inst. Technology, Stockholm, Sci. Report No. 18, 1967 (unpublished).
[20]*Handbook of Mathematical Functions*, edited by M. Abramowitz and I. A. Stegun, National Bureau of Standards, Appl. Math. Series 55 (U. S. GPO, Washington, D. C., 1964), p. 376.
[21]M. Sato, J. Phys. Soc. Japan 14, 1275 (1959).
[22]R. Barrie and R. R. Burgess, Can. J. Phys. 40, 1056 (1962).
[23]R. Stratton, Proc. Roy. Soc. (London) A246, 406 (1958).
[24]K. Blötekjaer, Arkiv Fysik 33, 105 (1966).
[25]Reference 1, p. 138 ff.
[26]V. L. Gurevich and Yu. A. Firsov, Zh. Eksperim. i Teor. Fiz. 40, 198 (1961) [Soviet Phys. JETP 13, 137 (1961)]; 47, 734 (1964) [20, 489 (1965)].

PHYSICAL REVIEW B VOLUME 2, NUMBER 10 15 NOVEMBER 1970

Electrical Properties of the GaAs X_{1C} Minima at Low Electric Fields from a High-Pressure Experiment

G. D. Fitt and J. Lees
Standard Telecommunication Laboratories Limited, London Road, Harlow, Essex, England
(Received 30 March 1970)

Hall-effect measurements at pressures extending to 60 kbar were made on single crystals of n-type GaAs grown by liquid epitaxy, vapor epitaxy, and bulk techniques over the carrier-concentration range 10^{13}–10^{19} cm^{-3} and with Se, Si, Sn, and Te dopants. The X_{1C} Hall mobility at 50 kbar for material in the 10^{14}–10^{17}-cm^{-3} range was 375 ± 45 cm^2/V sec after transfer from the Γ_{1C} minimum. [The labeling of states follows the notation of Wigner where the added subscripts C (as used in X_{1C}) and V (used in Γ_{15V}) refer to conduction- and valence-band states, respectively.] Extrapolation to atmospheric pressure gives a conductivity mobility of 328 ± 50 cm^2/V sec. Theoretical fits for the high-pressure data indicate a subband gap (X_{1C}-Γ_{1C}) of 0.38 ± 0.01 eV and a density-of-states ratio of $(N_x/N_\Gamma)_{P=0} = 45$, which implies X_{1C} density-of-states effective mass of $(0.85 \pm 0.10)m_e$. The loss of carriers at high pressures to impurity levels associated with the X_{1C} minima has been observed. The activation energies relative to the X_{1C} minima are estimated at 0.045 ± 0.01 eV for 10^{17}-cm^{-3} material with Si, Se, Te doping. Results have been analyzed in terms of the simple hydrogenic model. Ionized-impurity scattering in the X_{1C} minima has been shown to be unimportant for material with carrier concentrations below 10^{17} cm^{-3}.

I. INTRODUCTION

High-pressure experiments[1,2] were instrumental in determining the physical mechanism of the Gunn effect in GaAs. The threshold field for Gunn oscillations was found to decrease as the light-effective-mass Γ_{1C} [000] conduction band moved towards the heavy-effective-mass X_{1C} ⟨100⟩ conduction-band minima with pressure. This showed that the negative differential resistance which occurs near 3 kV/